AMERICAN SOCIETY FOR MICROBIOLOGY | Applied and Environmental Microbiology®

BIOTECHNOLOGY

Fluorescent Lead(IV) Sulfide Nanoparticles Synthesized by *Idiomarina* sp. Strain PR58-8 for Bioimaging Applications

Pallavee Srivastava, Meenal Kowshik

Department of Biological Sciences, Birla Institute of Technology and Sciences, Pilani, K K Birla Goa Campus, Zuarinagar, Goa, India

ABSTRACT The fabrication of nanoparticles by microorganisms presents a "green" method for generating biocompatible nanomaterials. We discovered the intracellular biosynthesis of fluorescent lead(IV) sulfide nanoparticles by the moderate halophile, *Idiomarina* sp. strain PR58-8. The bacterium tolerated up to 8 mM $Pb(NO_3)_2$ during growth. Non-protein thiols dose-dependently increased in response to metal exposure, which suggests they are involved in the growth of PbS_2 crystals and lead detoxification. Using X-ray diffraction, transmission electron microscopy (TEM), high-resolution TEM, and energy dispersive analysis of X-rays, the nanoparticles were characterized as spherical β-PbS_2 nanoparticles (PbS_2NPs) with a tetragonal crystal lattice, a crystallite domain size of 2.38 nm, and an interplanar distance of 0.318 nm. A narrow symmetric emission spectrum with a Gaussian distribution and an emission maximum at 386 nm was obtained when the particles were excited at 570 nm. The PbS_2NPs exhibited a large Stokes' shift (8,362 cm^{-1}) and a relatively high quantum yield (67%). These properties, along with fluorescence that was maintained in various microenvironments and their biocompatibility, make these nanoparticles excellent candidates for bioimaging. The particles were internalized by HeLa cells and evenly distributed within the cytoplasm, exhibiting their potential for *in situ* bioimaging applications. The "as-synthesized" lead(IV) sulfide nanoparticles may provide expanded opportunities for targeted bioimaging via modifying the surface of the particles.

IMPORTANCE This article reports the intracellular synthesis of fluorescent lead(IV) sulfide nanoparticles (PbS_2NPs) by a microorganism. All previous reports on the microbial synthesis of lead-based nanoparticles are on lead(II) sulfide that exhibits near-infrared fluorescence, requiring expensive instrumentation for bioimaging. Bioimaging using PbS_2NPs can be achieved using routine epifluorescence microscopes, as it fluoresces in the visible range. The research on PbS_2 nanoparticles to date is on their chemical synthesis employing toxic precursors, extreme pH, pressure, and temperature, resulting in cytotoxic products. In this context, the synthesis of PbS_2 nanoparticles by *Idiomarina* sp. strain PR58-8, described in this work, occurs at ambient temperature and pressure and results in the generation of biocompatible nanoparticles with no hazardous by-products. The excellent fluorescence properties that these particles exhibit, as well as their abilities to easily penetrate the cells and evenly distribute within the cytoplasm, make them exceptional candidates for bioimaging applications. This study demonstrated the synthesis and fluorescence bioimaging application of microbially synthesized PbS_2 nanoparticles.

KEYWORDS bioimaging, fluorescent, *Idiomarina*, lead(IV) sulfide, nanoparticles, halophiles

Received 10 November 2016 **Accepted** 14 January 2017

Accepted manuscript posted online 23 January 2017

Citation Srivastava P, Kowshik M. 2017. Fluorescent lead(IV) sulfide nanoparticles synthesized by *Idiomarina* sp. strain PR58-8 for bioimaging applications. Appl Environ Microbiol 83:e03091-16. https://doi.org/10.1128/AEM.03091-16.

Editor Maia Kivisaar, University of Tartu

Address correspondence to Meenal Kowshik, meenal@goa.bits-pilani.ac.in.

Nanotechnology is an interdisciplinary technology exploring the unique advantages of manipulating the structures of materials at the scales of individual atoms, molecules, and their organized aggregates (1). Nanofabrication results in materials with unique size-dependent, optical, physicochemical, electronic, mechanical, magnetic, and biological properties. These novel properties result from the large surface area-to-volume ratio, large surface energy, reduced imperfections, and spatial confinement of carriers/electrons. Over the last 3 decades, multidisciplinary efforts involving the interactions between researchers from the fields of physics, chemistry, materials science, mechanics, and biology have resulted in a substantial repertoire of nanoparticles and nanomaterials. Among these, the IV-VI family of lead-based semiconductor nanoparticles has garnered great attention in the past decade due to their size-tunable optical and electronic properties. These intrinsic properties make them excellent materials for diode lasers, optical detectors, solar cells, photoresistors, field-effect transistors, and biological applications, such as imaging and labeling (2, 3).

Among the lead-based semiconductor materials, lead(II) sulfide nanoparticles (PbSNPs), which exhibit a cubic crystallite lattice structure, a higher energy band gap ($>$0.41 eV), and size smaller than the exciton Bohr radius ($<$18 nm) of their bulk counterpart, are the most extensively studied (4). Although cubic PbSNPs and tetragonal lead(IV) sulfide nanoparticles (PbS_2NPs) exhibit similar properties, their ease of synthesis makes studies on PbSNPs more prevalent. The need for extreme conditions of temperature, pressure, and pH and the use of toxic precursors restrict studies on PbS_2 and PbS_2NPs (5, 6). The bulk synthesis of β-PbS_2 entails heating PbS with excess sulfur at temperatures higher than 650°C and a pressure of 30 kbars (5). Nano-particulate PbS_2 was first obtained as a by-product of synthesizing PbSNPs in natural zeolite at an ambient temperature and pressure via the hydrothermal process using the toxic precursor, thiourea. The formation of a β-PbS_2 crystalline phase was attributed to the selective nucleation within the special ordered structure of natural zeolite (7). β-PbS_2 thin films prepared by chemical bath and photochemical deposition methods employing an extreme pH exhibited p-type conductivity and a flower-like or oval morphology, respectively (8, 9). This brief background highlights the lacunae regarding the synthesis of and applications for PbS_2NPs. In this context, biological routes of nanoparticle synthesis present a "green" alternative, as the process occurs at an ambient temperature (room temperature/37°C) and pressure (760 mm Hg). Although the syntheses of PbSNPs by bacteria, fungi, and virus have been reported (10–14), there are no reports on the synthesis of PbS_2NPs by microorganisms.

Lead-based nanoparticles with a size distribution of 2 to 10 nm (quantum dots; QDs) have applications in near-infrared imaging (15–17). QDs exhibit size-tunable optical properties stemming from quantum confinement, negligible photobleaching due to narrow emission spectra, broad excitation spectra that enable multiphoton excitation, high quantum yields (QY), and a large Stokes' shift (18). These properties make the QDs excellent candidates for bioimaging and labeling applications, as the fluorescent dyes and proteins routinely used present several shortcomings, such as narrow excitation bands, broad emission spectra, small Stokes' shifts, low QYs, and photobleaching (16). However, a bottleneck for biological applications of QDs is their hydrophobicity and toxicity both *in vitro* and *in vivo* (15). Coating the QDs with hydrophilic moieties, such as thiolate ligand, silica, or other hydrophilic polymers, imparts them with hydrophilic and noncytotoxic properties (19, 20). Thus, an additional step of passivating/coating the QDs is required for biological applications. In this regard, the microbially synthesized nanoparticles are inherently coated with the biomolecule, which is most often responsible for their formation, circumventing the additional step required to make them amenable for biological applications (21, 22).

Here, we report the intracellular synthesis of noncytotoxic, biocompatible, tetragonal β-PbS_2 nanoparticles by the moderate halophile, *Idiomarina* sp. strain PR58-8. We characterized the nano-preparation by UV-visible spectroscopy, fluorescence spectroscopy, transmission electron microscopy (TEM), high-resolution TEM (HRTEM), selected area electron diffraction (SAED), and energy dispersive analysis of X-rays (EDAX). The

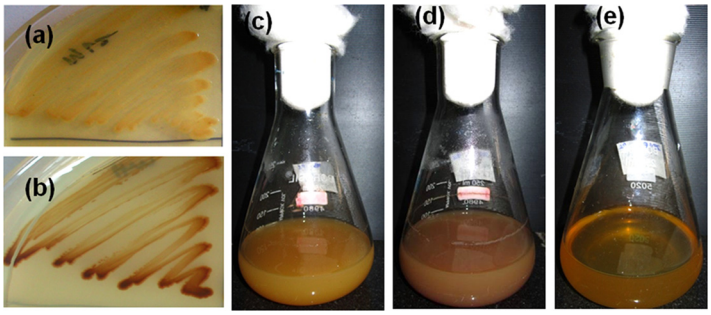

FIG 1 *Idiomarina* sp. strain PR58-8 appears golden yellow when grown in Zobell marine agar (a) and Zobell marine broth (c). In the presence of lead nitrate, it appears brown in color (b and d). Media controls with lead nitrate did not exhibit the brown coloration (e).

application of the "as-synthesized" nanoparticles as a bioimaging agent is also demonstrated. This may be the first report of synthesis of β-PbS_2 nanoparticles by microorganisms.

RESULTS

Effect of $Pb(NO_3)_2$ on the growth of *Idiomarina* sp. strain PR58-8. *Idiomarina* PR58-8 tolerated concentrations of $Pb(NO_3)_2$ as high as 8 mM in Zobell marine broth (ZMB) 2216 with a simultaneous change in appearance from golden yellow to brown (Fig. 1). The rates of growth at 0.05 and 0.5 mM $Pb(NO_3)_2$ were similar to that of the control [0 mM $Pb(NO_3)_2$]; however, a decrease in growth was observed with concentrations of $Pb(NO_3)_2$ higher than 1 mM (Fig. 2). The MIC of $Pb(NO_3)_2$ was 9 mM, as no growth was observed at this concentration. The moderate halophile exhibited a specific growth rate (μ) of 1.11 h^{-1}, with a doubling time (t_d) of 37.46 min and a lag time (t_l) of 30 min. In the presence of 0.05 mM and 0.5 mM $Pb(NO_3)_2$, the marine bacterium exhibited μ of 1.057 h^{-1} and 0.896 h^{-1}, respectively, neither of which was significantly different from the control ($P > 0.05$). Similarly, the differences between the t_d and t_l of the cells grown in the presence of 0 mM (control), 0.05 mM, and 0.5 mM $Pb(NO_3)_2$ were not significant (Table 1). However, in the presence of 1 mM and 5 mM $Pb(NO_3)_2$, the specific growth rates were 0.690 h^{-1} and 0.463 h^{-1}, respectively, which were significantly lower ($P < 0.05$) than the control. The t_d and the t_l for cells grown in the presence of 1 mM and 5 mM $Pb(NO_3)_2$ were significantly higher ($P < 0.05$).

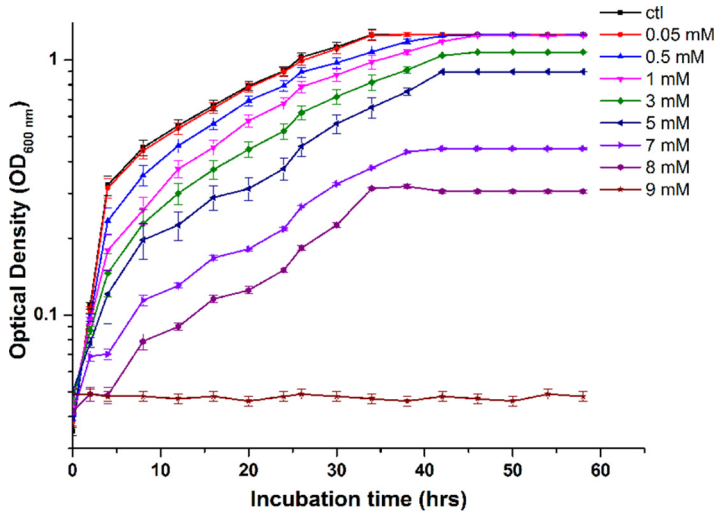

FIG 2 Growth profile of *Idiomarina* PR58-8 at various concentrations of $Pb(NO_3)_2$. The MIC of $Pb(NO_3)_2$ was 9 mM. Values on the *y* axis are presented in $\log_{10}$ scale and are means ± SE (error bars) for three experiments.

TABLE 1 Growth kinetics of *Idiomarina* sp. strain PR58-8 in the absence and presence of lead nitrate

Parameter[a]	Concn. of $Pb(NO_3)_2$ (mM)				
	0 (control)	0.05	0.5	1	5
μ (h^{-1})	1.110 ± 0.019	1.057 ± 0.013	0.896 ± 0.018	0.690 ± 0.016	0.463 ± 0.015
t_d (min)	37.46 ± 0.008	39.34 ± 0.011	46.41 ± 0.009	60.26 ± 0.015	89.81 ± 0.019
t_l (min)	30 ± 0.011	30 ± 0.015	45 ± 0.013	60 ± 0.007	120 ± 0.023

[a]μ, specific growth rate; t_d, doubling time; t_l, lag time.

Nanoparticle synthesis and Pb uptake. When grown in the presence of $Pb(NO_3)_2$, *Idiomarina* PR58-8 exhibited an intracellular accumulation of lead, with a concomitant loss of lead from the medium, beginning from early exponential phase (6 h) through late stationary phase (42 h). For cells grown in the presence of 0.5 mM (103.63 μg/ml) $Pb(NO_3)_2$, the Pb concentration in the medium at 6 h was 87.35 μg/ml, and only ~1.7% (1.8 μg/ml) remained unutilized in the medium by 42 h. There was no loss of lead observed in the negative control [culture-free medium with 5 mM $Pb(NO_3)_2$] throughout the course of the experiment (data not shown). In the case of cells grown in the presence of 5 mM (1036.29 μg/ml) $Pb(NO_3)_2$, only 0.8% (9.24 μg/ml) remained unutilized by 42 h. In both instances, *Idiomarina* PR58-8 accumulated ~91% of the lead by 36 h (Fig. 3).

The growth of *Idiomarina* PR58-8 in the presence of $Pb(NO_3)_2$ was accompanied by a change in color of the golden yellow culture to brown (Fig. 1). The culture supernatant and the medium controls without inoculum did not show this color change. The time course of lead uptake and nanoparticle yield correlated with the growth phase of *Idiomarina* PR58-8 (Fig. 3). The yields with respect to biomass and substrate added were estimated along with the efficiency of the process (Table 2). Yields (with respect to substrate added) of 0.902 mg/mg Pb and 0.965 mg/mg Pb were obtained in the presence of 0.5 and 5 mM $Pb(NO_3)_2$, respectively, at 54 h. The process had efficiencies of 90.3% and 96.5% in the presence of 0.5 and 5 mM $Pb(NO_3)_2$, respectively. As the yield with respect to biomass in the presence of 5 mM $Pb(NO_3)_2$ (631.71 μg/mg [dry weight] cells) was significantly higher ($P < 0.05$) than the yield (60.4 μg/mg [dry weight] cells) obtained in the presence of 0.5 mM $Pb(NO_3)_2$, the synthesis was carried out at 5 mM $Pb(NO_3)_2$.

Thiol assay. The intracellular thiol concentrations of the cells exposed to various concentrations of $Pb(NO_3)_2$ were estimated over a period of 60 h to determine the roles of thiols in metal chelation, resistance, and/or transformation. At 6 h, nonprotein thiols (NP-SH) accounted for 88.3% in untreated controls, while protein-bound thiols (PB-SH)

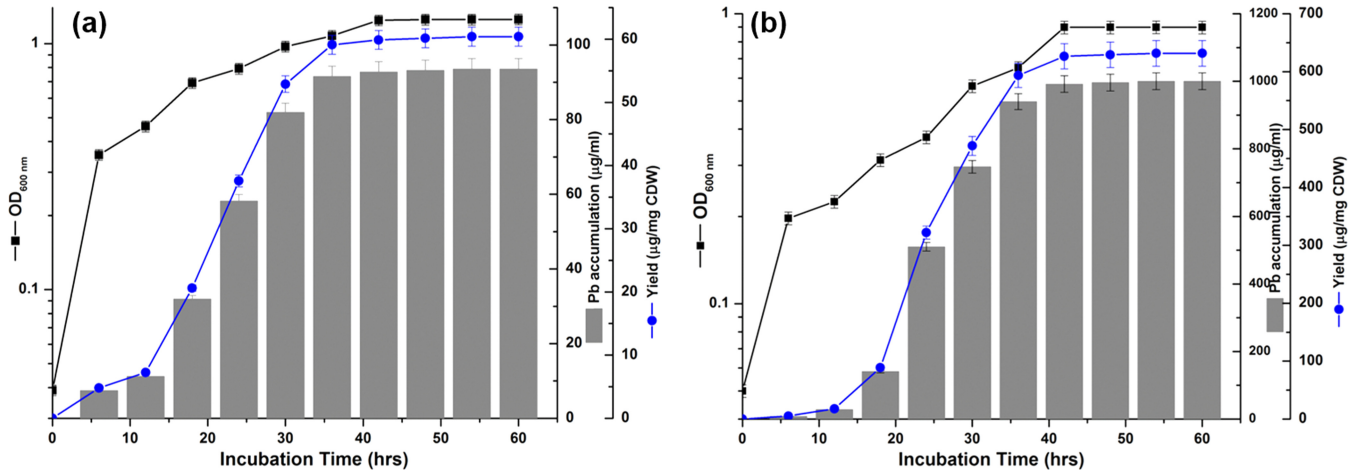

FIG 3 Growth kinetics, lead accumulation, and the yield of lead-based nanoparticles when *Idiomarina* PR58-8 was grown in the presence of 0.5 mM $Pb(NO_3)_2$ (a) and 5 mM $Pb(NO_3)_2$ (b). Values on the *y* axis are presented in $\log_{10}$ scale and are means ± SE (error bars) for three experiments. CDW, cells (dry weight).

TABLE 2 Yields of the lead-based nanoparticles synthesized by *Idiomarina* sp. strain PR58-8

Parameter	Concn. of $Pb(NO_3)_2$ (mM)	
	0.5	5
Yield (μg/mg CDW)[a]	60.4 ± 0.015	631.71 ± 0.017
Molar yield (mg/mg Pb)	0.902 ± 0.011	0.965 ± 0.014
Efficiency (%)	90.3	96.5

[a]CDW, cell dry weight.

accounted for 11.7% of the total thiols (T-SH). However, at 60 h, PB-SH increased to 70.9% while NP-SH decreased to 29.1%. On the other hand, $Pb(NO_3)_2$-exposed cells exhibited dose-dependent and time-dependent increases in NP-SH (Fig. 4a). The NP-SH was ~4 times higher in cells treated with 5 mM $Pb(NO_3)_2$ than in untreated controls, while the PB-SH decreased ~1.05 times compared with that in controls at 36 h. Simultaneous increases in the intracellular lead and NP-SH concentrations were observed at 18 h, suggesting a positive interdependence between the two (Fig. 4b and c). The increase in T-SH as a function of the increase in NP-SH is evident in Fig. 4a.

Characterization of lead-based nanoparticles. X-ray diffraction (XRD) spectra of the "as-synthesized" nanoparticles revealed peaks characteristic of tetragonal lead(IV) sulfide (PbS_2) corresponding to the International Centre for Diffraction Data (ICDD) card no. 20-0596 (Fig. 5a). A broadening of the peaks at the base is indicative of the particles being nano-sized. The crystallite domain size as calculated using the Debye-Scherrer formula for a (2 0 0) peak was 2.38 nm. The lattice parameters for tetragonal system were a = 4.45 Å and c = 4.24 Å. UV-visible spectroscopy of the "as-synthesized" PbS_2NPs revealed an absorbance maximum (λ_{abs}) at 386 nm (Fig. 5b), corresponding to a band gap energy of ~3.22 eV. The morphology of the nanoparticles was characterized by transmission electron microscopy (TEM) and high resolution-TEM (HRTEM). TEM

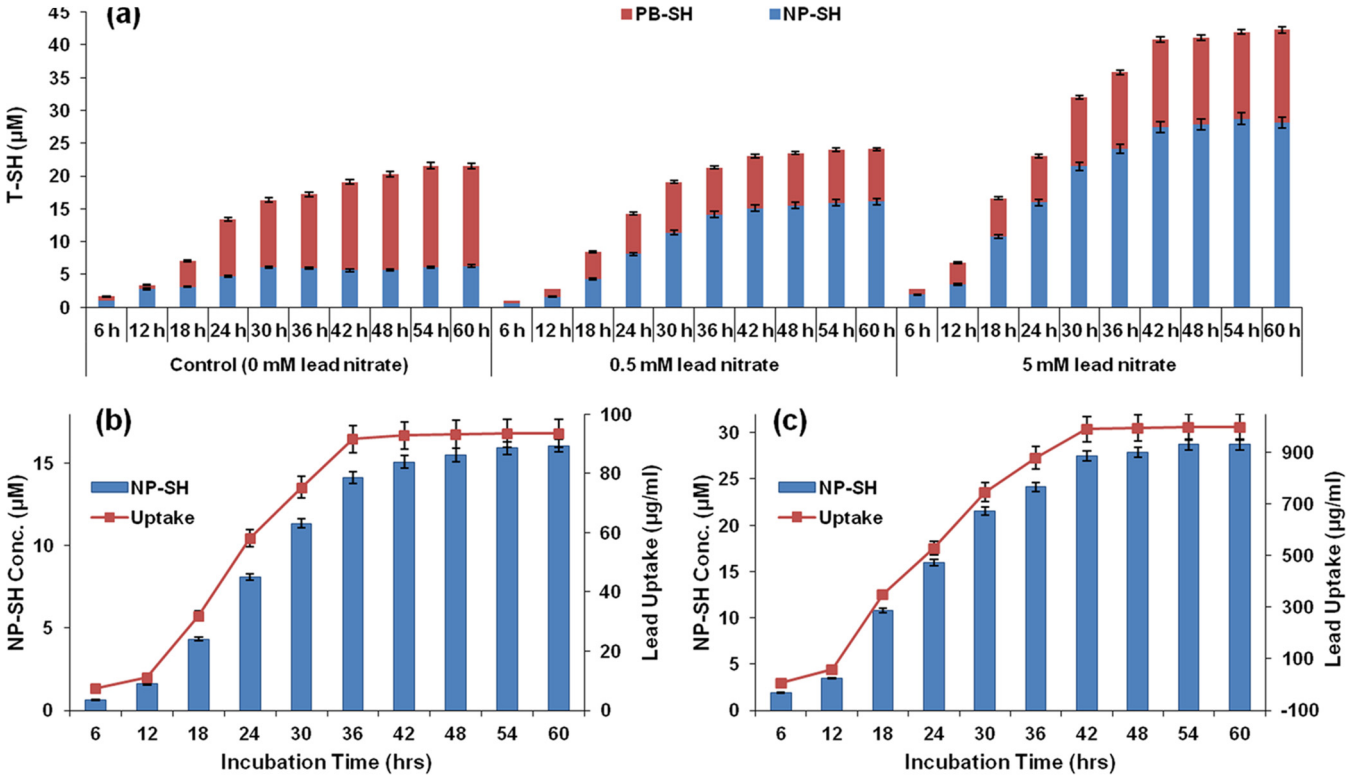

FIG 4 (a) Effect of lead nitrate on the intracellular levels of total thiols (T-SH), non-protein thiols (NP-SH), and protein-bound thiols (PB-SH) with respect to time. A dose-dependent increase in NP-SH was observed in response to lead stress. The increasing NP-SH concentrations corresponded to the lead uptakes exhibited by *Idiomarina* PR58-8 in the presence of 0.5 mM $Pb(NO_3)_2$ (b) and 5 mM $Pb(NO_3)_2$ (c). Values are means ± SE (error bars) for three experiments.

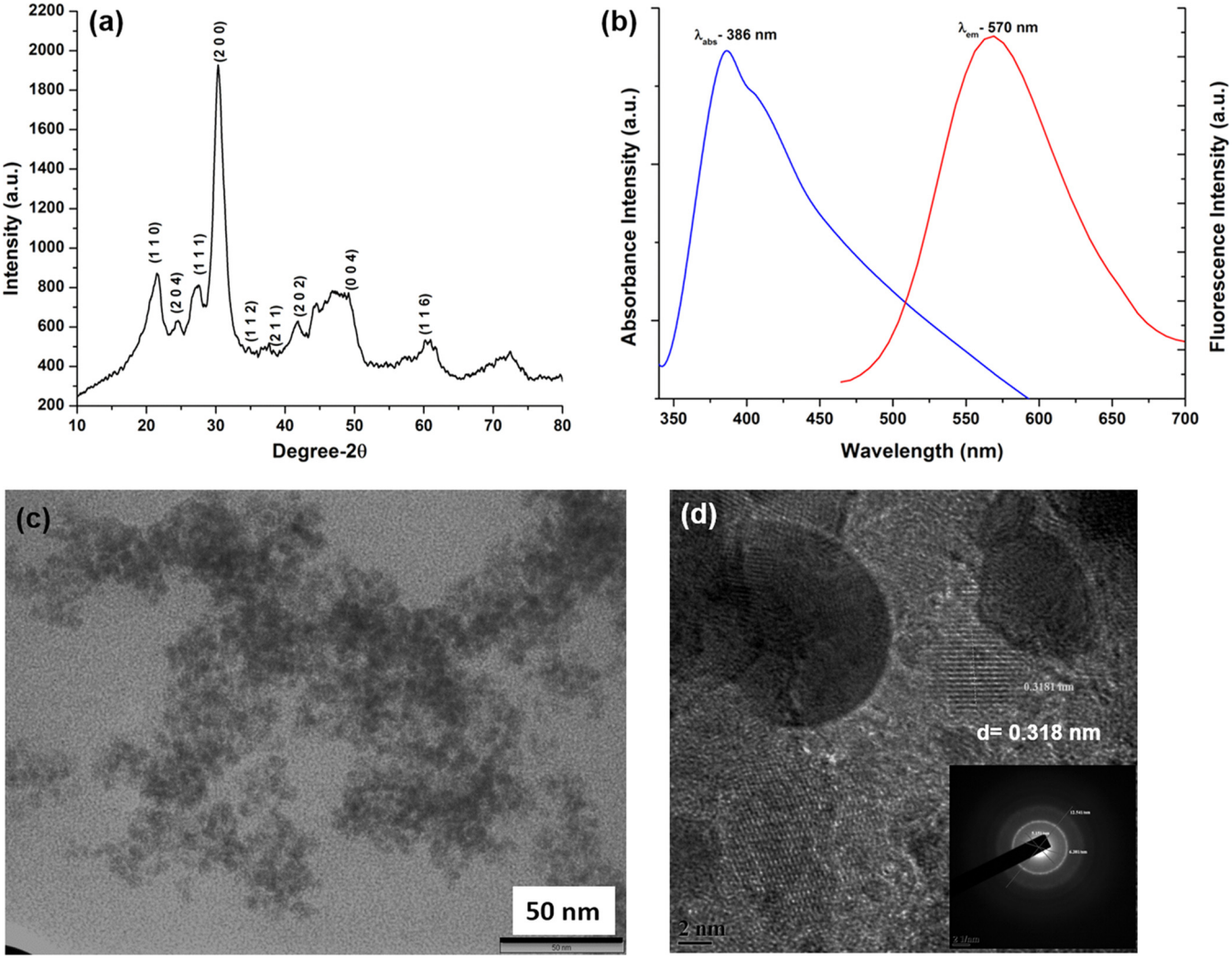

FIG 5 Characterization of PbS_2NPs synthesized by *Idiomarina* PR58-8. (a) XRD spectrum exhibiting the Bragg's peak characteristic for tetragonal PbS_2. (b) The absorbance and the emission spectra showing an absorbance maximum at 386 nm and an emission maximum at 570 nm. (c) TEM micrographs revealing spherical particles with an average size of 6 nm. (d) HRTEM micrograph showing a phase image of the particles with interplanar spacing of 0.318 nm. (d, inset) SAED pattern corresponding to the tetragonal crystal facets, where the three (inner, middle, and outer) rings could be indexed to Bragg's planes of (1 1 1), (2 0 4), and (2 0 0). The inner ring diameter is 5.15 1/nm [corresponding to the (1 1 1) plane], the middle ring diameter is 6.38 1/nm [corresponding to the (2 0 4) plane], and the outer ring diameter is 12.54 1/nm [corresponding to the (2 0 0) plane].

analysis indicated the presence of particles with a spherical morphology with an average size of 6 nm (Fig. 5c). An image from HRTEM of the "as-synthesized" PbS_2NPs revealed nearly spherical particles with an average size of 6 nm, and interplanar spacing (*d*) of 0.318 nm (Fig. 5d), which corresponds to the *d*-spacing of the (2 0 0) plane [$d_{(2\ 0\ 0)}$ = 0.307 nm of ICDD card no. 20-0596]. The SAED pattern of the PbS_2NPs (Fig. 5d inset) indexes to the tetragonal PbS_2 crystallite planes of (2 0 0), (1 1 1), and (2 0 4). Fast Fourier transform (FFT) analysis of the PbS_2NPs was also carried out to obtain the diffraction pattern and to measure the distances between the atomic planes. The elemental composition of the PbS_2NPs as determined by EDAX showed overlapping peaks for Pb and S at 2.3 keV, confirming their presence.

The photoluminescence (PL) spectra of the PbS_2NPs showed an emission maximum (λ_{em}) at 570 nm (Fig. 5b). The storage of samples for 6 months at room temperature either as a powder or as a colloidal suspension did not have any effect on the fluorescence spectra of the PbS_2NPs (Fig. 6a). The PL spectrum for lyophilized cellular material of *Idiomarina* PR58-8 (ML2) did not exhibit a λ_{em}, but instead, luminescence was observed over a broad range (~340 nm to 500 nm), which disappeared after

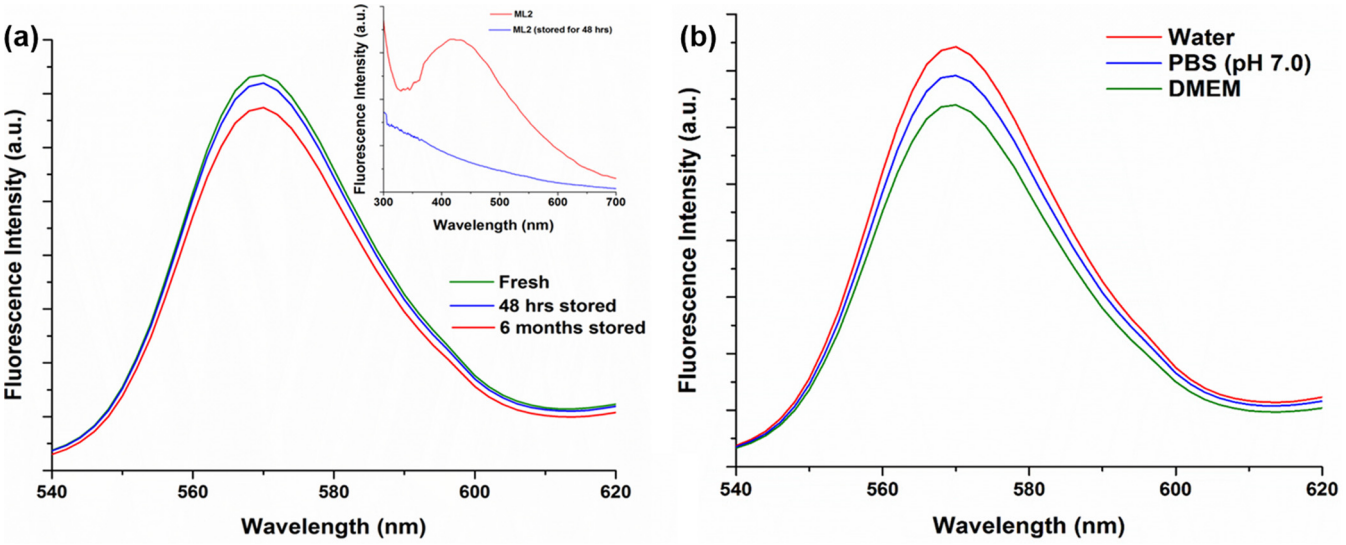

FIG 6 (a) Effect of storage on the emission spectra of the PbS_2NPs synthesized by *Idiomarina* PR58-8. Even after a storage of 6 months, the emission spectrum of the PbS_2NPs was similar to that of fresh PbS_2NPs, with a λ_{em} at 570 nm. (a, inset) The photoluminescence spectra of the lyophilized *Idiomarina* PR58-8 exhibiting a broad peak, which disappeared after a storage of 48 h. (b) The fluorescence spectra of PbS_2NPs synthesized by *Idiomarina* PR58-8 in solvents, such as water, PBS (pH 7.0), and DMEM.

storage for 48 h or more (Fig. 6a inset). The PL spectra of the PbS_2NPs recorded in phosphate-buffered saline (PBS [pH 7.0]) and Dulbecco's modified eagle medium (DMEM) did not exhibit any changes in the fluorescence (Fig. 6b). The λ_{em} of the PbS_2NPs exhibited a Stokes' shift of 8,362 cm^{-1} (184 nm). The QYs of the synthesized PbS_2NPs were 0.67 in each of the three solvents.

Biocompatibility studies, internalization, and bioimaging. The biocompatibility of the PbS_2NPs was evaluated in the HeLa cell line using the 3-(4,5-dimethyl-2-thiazolyl)-2,5-diphenyl-2H-tetrazolium bromide (MTT) assay. Even at the highest concentration of PbS_2NPs (50 μg/ml or 0.21 mM), viabilities of 90.31% and 88.77% were observed after 24 and 48 h of treatment, respectively (Fig. 7a). The nanoparticles exhibited no significant ($P > 0.05$) difference in viability compared with that of untreated controls at either of the time points. Similarly, ML2 did not exhibit any significant cytotoxicity at any of the concentrations tested. On the other hand, $Pb(NO_3)_2$ showed significantly higher ($P < 0.05$) toxicity toward HeLa cells at concentrations of 20 μg/ml (0.06 mM) and higher (Fig. 7a). A similar trend was observed with respect to the generation of reactive oxygen species (ROS), wherein the "as-synthesized" PbS_2NPs

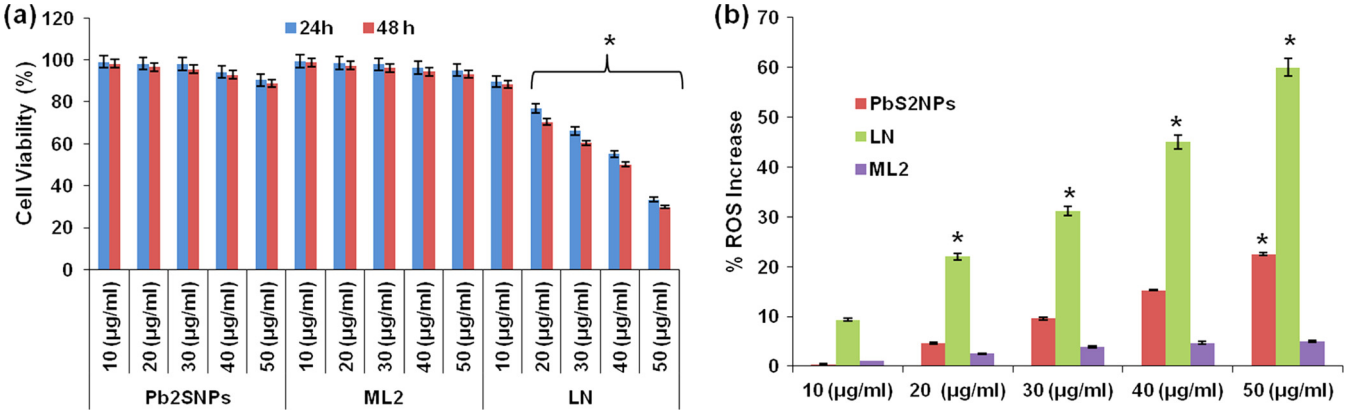

FIG 7 (a) Effect of PbS_2NPs, lead-free cell material (ML2), and lead nitrate (LN) on viability of HeLa cells. The PbS_2NPs and ML2 did not exhibit toxicity against HeLa cells. LN dose-dependently decreased cell viability. (b) Effect of PbS_2NPs, ML2, and LN on ROS generation in HeLa cells. PbS_2NPs and ML2 did not significantly increase ROS production, except for 50 μg/ml (0.21 mM) PbS_2NPs, which significantly increased ROS. LN dose-dependently increased ROS generation, which became significant at 20 μg/ml (0.13 mM). Values are means ± SE (error bars) for three experiments. *, $P < 0.05$.

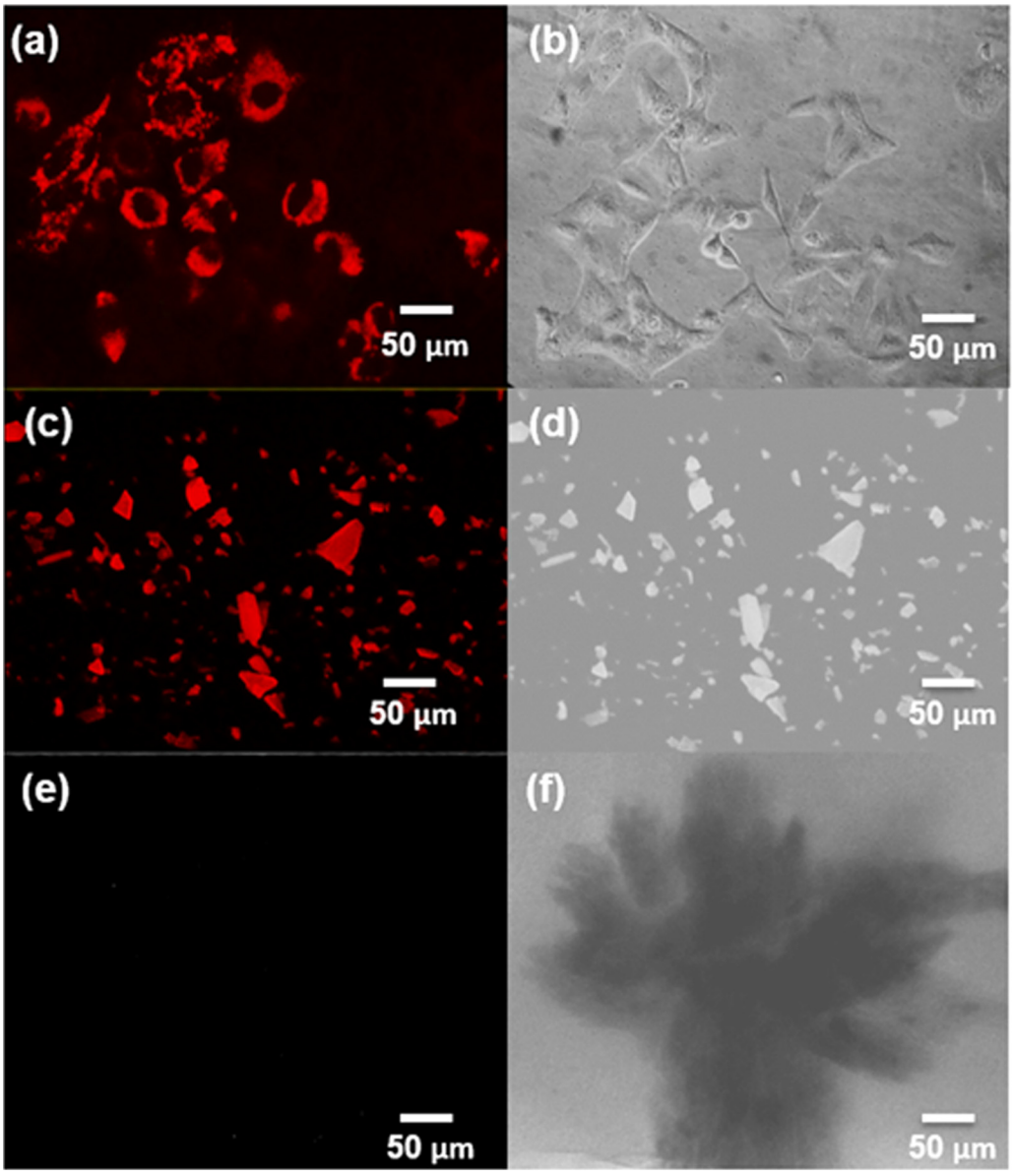

FIG 8 (a) Fluorescence micrograph of HeLa cells stained with 30 μg/ml (0.13 mM) PbS_2NPs. The nanoparticles exhibited red fluorescence, were evenly distributed in the cytoplasm, and did not stain the nuclei. (b) Phase contrast micrograph of HeLa cells treated with 30 μg/ml (0.13 mM) PbS_2NPs. (c) Fluorescence micrograph of powdered PbS_2NPs. (d) Phase contrast micrograph of powdered PbS_2NPs. (e) Fluorescence micrograph of the lyophilized *Idiomarina* PR58-8. (f) Phase contrast micrograph of the lyophilized *Idiomarina* PR58-8.

at 40 μg/ml (0.17 mM) did not show a significant increase ($P > 0.05$) in ROS (Fig. 7b), while at 50 μg/ml (0.21 mM), the increase was significant (23%; $P < 0.05$). No ROS production was observed in ML2-treated cells, whereas HeLa cells exposed to $Pb(NO_3)_2$ exhibited a dose-dependent increase in ROS (Fig. 7b). At 10 μg/ml (0.03 mM) $Pb(NO_3)_2$, the increase in ROS was not significant ($P > 0.05$) but reached significance ($P < 0.05$) at concentrations of 20 μg/ml (0.06 mM) and higher. Similar studies were carried out for a model normal cell line, human epidermal keratinocytes (HaCaT cells), where PbS_2NPs did not exhibit toxicity at up to 50 μg/ml or 0.21 mM (data not shown).

HeLa cells grown in the presence of 30 μg/ml (0.13 mM) PbS_2NPs were observed under an epifluorescence microscope using the tetramethyl rhodamine isocyanate (TRITC) filter to check for internalization of the nanoparticles and for bioimaging. Figure 8a shows cells with internalized PbS_2NPs that appear as red fluorescent particles. Figure 8c shows an image of the PbS_2NPs powder exhibiting red fluorescence,

while the lead-free lyophilized cellular material, ML2 (Fig. 8e), did not exhibit any fluorescence. Figure 8b, d, and f show phase-contrast images of PbS_2NPs-treated cells, PbS_2NPs, and ML2, respectively. A corrected total cell fluorescence (CTCF) analysis of the cells stained with PbS_2NPs showed fluorescence intensity was directly proportional to the size of the cell.

DISCUSSION

Idiomarina sp. strain PR58-8 is a moderate halophile, with a requirement for 1% NaCl and can tolerate up to 15% NaCl (23). This strain possesses a high level of intrinsic resistance to silver ions (23) and selenium oxyanions (24). The marine bacterium also exhibited a high resistance to $Pb(NO_3)_2$, as is evident from the MIC value (Fig. 2). The growth kinetics were not affected up to a concentration of 0.5 mM $Pb(NO_3)_2$, although a slight decrease was observed at concentrations greater than 1 mM (Table 1). Growth in the presence of $Pb(NO_3)_2$ was accompanied by a change in coloration of the culture from yellow to brown (Fig. 1), indicating the transformation of the metal salt to a lead-based nano-particulate product.

The marine bacterium accumulated lead from early exponential phase to late stationary phase (Fig. 3), a finding in contrast to the lead uptake exhibited by the yeasts associated with PbSNPs synthesis, *Rhodosporidium diobovatum* and *Torulopsis* sp. (11, 13). Lead accumulation in both of these yeasts was observed from mid-exponential phase up to late stationary phase (11, 13). The presence of anions, such as chloride (3.1%), sulfate (0.32%), and phosphate (0.0008%), in the culture medium may chelate the Pb^{2+} ions to form insoluble or poorly soluble lead compounds, giving a false positive for uptake studies. In the presence of Cl^- and SO_4^{2-} ions, Pb preferentially forms chloride salts that are readily available for uptake, and the small amount of soluble $PbSO_4$ formed is also available (25). The trace amounts of $Pb_3(PO_4)_2$ formed are available for uptake between a pH of 6.0 and 7.5 (26). The growth of *Idiomarina* PR58-8 to early exponential phase results in a decrease in the pH of ZMB from 7.5 to 6.0. The lowering of the pH results in dissolution of the poorly soluble lead salts, making them available for uptake. The effects of the time at which the $Pb(NO_3)_2$ was added on the growth of *Idiomarina* PR58-8 and the synthesis of nanoparticles was determined by introducing $Pb(NO_3)_2$ at the time of inoculation (0 h) or at early exponential phase (6 h). The addition of $Pb(NO_3)_2$ at 0 h did not affect the growth of *Idiomarina* PR58-8, but was accompanied by changes in the coloration of the culture and nanoparticle synthesis. When the $Pb(NO_3)_2$ was introduced in the early exponential phase, the growth rate was reduced, with no associated color change. However, growth resumed when these cells were transferred to fresh ZMB 2216 without $Pb(NO_3)_2$, suggesting that the introduction of $Pb(NO_3)_2$ during the early exponential phase was bacteriostatic and not bactericidal. The adaptation for growth in the presence of $Pb(NO_3)_2$ added at the time of inoculation may be attributed to the intrinsic metal-resistance mechanisms of the culture and the decreased availability of Pb^{2+} ions to the bacterial cells. Fresh ZMB medium has a pH of 7.5, which decreases to ~6.0 in the early exponential phase. The solubility of lead complexes is higher at pH 6.0, which corresponds to increased concentrations of free Pb^{2+} ions and more toxicity (27). Between pH 6.5 and 7.5, fewer Pb^{2+} ions are available. Therefore, the addition of $Pb(NO_3)_2$ at the time of inoculation may not hinder the growth of *Idiomarina* PR58-8 while allowing the bacteria to slowly adapt to the Pb^{2+} ion concentration. Thus, $Pb(NO_3)_2$ was added simultaneously with the inoculum. This is an advantage exhibited by the marine bacterium over the yeasts, *Torulopsis* sp. and *R. diobovatum*, which require the addition of $Pb(NO_3)_2$ at mid-log phase for the synthesis of PbSNPs (11, 13), as it circumvents the need for growth phase monitoring.

The change in coloration we observed during the growth of *Idiomarina* PR58-8 in the presence of $Pb(NO_3)_2$ (Fig. 1) was not observed when the metal salt was added to the culture supernatant or medium control, indicating that the intracellular synthesis of the lead-based nanoparticles was a culture-dependent phenomenon. The synthesis of lead-based nanoparticles by *Idiomarina* PR58-8 was more efficient at 5 mM $Pb(NO_3)_2$,

as evident from the yield of the particles both with respect to biomass and substrate (Table 2).

The synthesis of metal-based nanoparticles by microbes usually involves the metal detoxification mechanisms intrinsic to the bacteria. As the Pb^{2+} ion offers limited beneficial functions to eukaryotes and prokaryotes, it is considered a toxin (28). Thus, microbes have evolved numerous mechanisms to overcome the stress exerted by the lead cation. Microorganisms may prevent the influx of Pb^{2+} ions by either precipitating it as an insoluble phosphates or by adsorption on the cell wall via exopolysaccharides (EPS) and/or other cell wall components. If the Pb^{2+} ion is taken up by the microbial cell, it may be sequestered as a phosphate or effluxed out of the cell via transporters *viz*., CadA, ZntA, and PbrA (29). Pb^{2+} ions can also be rendered inactive by thiol compounds that include non-protein thiols (NP-SH), such as glutathione (G-SH), cysteine, and cystine. and protein-bound thiols (PB-SH), such as phytochelatins, and metallothioneins (30, 31). In the presence of metal ions, such as lead, bacteria and fungi increase the cellular pools of thiols, thereby sequestering the toxic ions (32). *Idiomarina* RR58-8, a *Gammaproteobacteria*, has G-SH as the most abundant thiol (33). Thus, the involvement of thiols in lead resistance and transformation was investigated. The marine bacterium exhibited a dose-dependent increase in NP-SH with concomitant decrease in PB-SH in the presence of lead nitrate (Fig. 4). A similar trend was reported in response to various metals, such as Pb, Ag, Cd, and Zn, in bacteria and fungi (11, 23, 34), which may be attributed to the presence of metal ions that cause the sulfur in the proteome to be redirected toward G-SH synthesis (35). Although the lead uptake during the growth of *Idiomarina* PR58-8 commenced from early exponential phase (6 h), active uptake began at only around 18 h, at which time the concentration of NP-SH within the lead-exposed cells also increased. The increase in NP-SH concentration continued until the late stationary phase (42 h) and corresponded to the lead uptake profile (Fig. 4b and c). Our results suggest the involvement of NP-SH in lead resistance and the synthesis of lead-based nanoparticles.

The "as-synthesized" nanoparticles exhibited a tetragonal crystal lattice of lead(IV) sulfide nanoparticles (Fig. 5a). This is the first report on the synthesis of PbS_2 nanoparticles by a microorganism. Previous reports on the fabrication of tetragonal PbS_2 nanoparticles were via a chemical synthesis route (7–9, 36). The α (hexagonal) and β (tetragonal) PbS_2 phases are considered high-pressure phases, as their synthesis requires pressures higher than 20 kbars and temperatures higher than 600°C (5). The synthesis of PbS_2 at atmospheric pressure in natural zeolite was attributed to the ordered structure of the porous matrix acting as the nucleation centers leading to the generation of compressed lead sulfide phases (7). A similar nucleation, with biomolecules of bacterial origin acting as the center, may be responsible for the generation of β-PbS_2 nanoparticles by *Idiomarina* PR58-8. The extracellular syntheses of PbSNPs by bacteria, fungi, and yeasts (10–13) may not provide the enclosed environment for the biomolecules to act as nucleation centers, preventing the synthesis of a compressed form of PbS. On the other hand, the synthesis of compressed lead sulfide phases (PbS_2NPs) in our study may be attributed to the intracellular synthesis, which provides an environment appropriate for the nucleation of PbS_2. The small crystallite domain size of the "as-synthesized" nanoparticles may be responsible for the tetragonal crystal lattice. Qadri et al. (36) attributed the formation of the tetragonal lattice structure during synthesis in the bicontinuous cubic phase of a lipid to the distortion in the cubic lattice of the lead sulfide nanocrystallites when the crystallite size decreased to $<$6 nm. The PbS_2NPs exhibited an a/c ratio of 1.05, which corresponds to the a/c ratio obtained for tetragonal PbS nanocrystallites of $\sim$3 nm (36).

UV-visible spectroscopy showed an absorbance maximum in the visible range (Fig. 5b) with an energy band gap of $\sim$3.22 eV. Roman-Zamorano et al. (7) attributed the shift in the λ_{abs} of PbSNPs from 240 nm to $\sim$400 nm to the heating at/above temperatures of 55°C resulting in the generation of PbS_2NPs. The thin films of PbS_2NPs synthesized via chemical routes exhibit a similar λ_{abs} at $\sim$400 nm (8). On the other hand, the λ_{abs} of the PbSNPs synthesized by *Torulopsis* sp. and *R. diobovatum* were 330

nm and 320 nm, respectively (11, 13). The blue shift of the absorbance spectra is a result of the particle size becoming smaller than the excitonic Bohr radius of the bulk PbS (quantum confinement) (4). The nano-preparation exhibited a spherical morphology and narrow size distribution, as evident from TEM/HRTEM micrographs (Fig. 5c and d), which may be attributed to the kinetic constraints imposed by the strong binding conditions within the bacterial cells (7). Similar spherical PbS_2NPs with an average size of ~10 nm stabilized in natural zeolite have been reported (7). An elemental analysis confirmed the presence of Pb and S; the peaks of S overlap with that of Pb, and both peaks appear at 2.3 keV (35).

The emission spectra of the "as-synthesized" PbS_2NPs exhibited a Gaussian spectral line shape with a full width at half maximum (FWHM) of 24.09 nm (Fig. 5b). A majority of the semiconducting QDs exhibit Gaussian emission spectra with FWHMs of ~30 nm that confer the QDs with multiplexing capabilities (16). To eliminate the possibility of the observed florescence arising due to the bacterial cells or any of their components, the lead-free cell material (ML2) was also evaluated for its fluorescent properties. ML2 exhibited luminescence (Fig. 6a inset), which may be attributed to the presence of biomolecules, such as NADH and tryptophan (13). However, after 48 h of storage at room temperature as is or in water/PBS, the luminescence disappeared due to the degradation of these biomolecules (37, 38). On the other hand, storage had no effect on the fluorescence spectra of the PbS_2NPs (Fig. 6a). Similarly, varying the solvent (DMEM or PBS) also did not alter the fluorescence spectra, where DMEM was used to mimic the *in vitro* environment and PBS was used to mimic the extracellular environment (Fig. 6b). Thus, these PbS_2NPs are capable of retaining their fluorescent property in various environments. Most of the chemically synthesized PbS quantum dots have emissions in the near-infrared region (NIR) (17, 39, 40), with the exception of PbS colloids synthesized by controlled precipitation in water and acetonitrile solutions that exhibit λ_{em} in the visible range (41). These PbS colloids were shown to have a λ_{em} of 436 nm and/or 600 nm based on their size, with an excitation wavelength of 355 or 410 nm, respectively (41). Since the λ_{em} of the PbS_2NPs synthesized by *Idiomarina* PR58-8 is in the visible range, it is advantageous as routine, relatively inexpensive epifluorescence microscopes can be easily used for bioimaging.

Biological imaging requires sensitive fluorophores with relatively large Stokes' shifts and acceptable QYs. The Stokes' shift, defined as the red shift of the emission spectra with respect to the absorption spectra, should be on the order of 5,000 to 10,000 cm^{-1} for an efficient fluorescent stain (42). QY, an intrinsic property of fluorescent probes, is defined as the ratio of the number of emitted photons to the absorbed photon. The PbS_2NPs exhibited a large Stokes' shift with a relatively high quantum yield (67%). The QY of the particles was estimated using the reference dye coumarin 153 (QY, 58%), which has a λ_{abs} at 422 nm and a λ_{em} at 531 nm. The QY of PbS quantum dots synthesized by various chemical methods has been reported to be between 10 to 90% based on their size (43). The PbS_2NPs synthesized by *Idiomarina* PR58-8 exhibited narrow symmetric emission spectra with a Gaussian distribution, and a λ_{em} in the visible range with a large Stokes' shift and relatively high QY. Moreover, they were not affected by their microenvironment and thus, present a fluorophore superior to organic dyes for bioimaging applications.

Biocompatibility and noncytotoxicity are prerequisites for the use of a fluorophore as a bioimaging agent. The PbS_2NPs did not exhibit toxicity toward HeLa cells at any of the concentrations tested (Fig. 7a). Similarly, ML2 did not exhibit cytotoxicity, whereas, at concentrations greater than 20 μg/ml (0.06 mM), lead nitrate was found to be toxic to HeLa cells. Similar results were reported for human leukemia (HI-60) cells treated with lead nitrate (44). This speaks in favor of the biocompatibility of PbS_2NPs compared with that of $Pb(NO_3)_2$. Lead nitrate exerts cytotoxicity by inducing oxidative stress as a result of ROS generation followed by the depletion of the antioxidative reserves (45). Thus, to further assess the biocompatibility of PbS_2NPs, the ROS assay was carried out on HeLa cells treated with the nano-preparation. The PbS_2NPs did not increase ROS generation (Fig. 7b). Lead-based nanoparticles obtained through chemical

routes of synthesis are cytotoxic and require further treatment with capping agents to make them biocompatible (17, 38). Previous studies have shown that functionalizing/capping agents may affect the cytotoxicity of the particles either way, as certain agents, such as 3-mercaptopropane sulfonate and sodium 2,3-dimercaptopropane sulfonate, were found to make the particles more toxic, while others, *viz*., β-lactoglobulin, glutathione, and DNA, rendered them nontoxic (17, 38, 46). Pb in its divalent cationic form (Pb^{2+}) disrupts various physiological functions by replacing divalent cations, such as Ca^{2+}, Mg^{2+}, and Fe^{2+}, and sometimes monovalent cations, such as Na^{+}, present in the biological system (47). Capping the PbS QDs with stabilizing molecules, such as G-SH or β-lactoglobulin, prevents the release of Pb^{2+}, thereby attenuating the cytotoxicity of the QDs (16). Pb in the PbS_2NPs synthesized by *Idiomarina* PR58-8 is in a 4+ oxidation state (PbS_2), and the particles are most likely capped by a thiol containing proteinaceous biomolecules accounting for ~10% of the total particles (data not shown). The capping agents stabilizing the nanoparticles prevent exposure of the Pb^{4+} ion to the reducing moieties present in the biological environment and its reduction to Pb^{2+}, thereby lowering its toxicity. Thus, PbS_2NPs synthesized by *Idiomarina* PR58-8 were found to be biocompatible and may be deemed safe for bioimaging applications.

The PbS_2NPs exhibited red fluorescence when observed under the TRITC filter of the epifluorescence microscope. The particles did not penetrate the nucleus and were evenly distributed within the cytoplasm of the cell (Fig. 8a). The CTCF (corrected total cell fluorescence) data indicate a uniform distribution of the particles. Hence, these PbS_2NPs may be used as *in situ* fluorescent probes. The "as-synthesized" PbS_2NPs may also be used for targeted biolabeling, where the nanoparticles can be functionalized to target a specific subset of cells. As the PbS_2NPs synthesized by *Idiomarina* PR58-8 are most likely capped with NP-SHs, the preparation can be suitably modified at the SH site by attaching various targeting ligands and antibodies for site-directed imaging. Thus, the "as-synthesized" PbS_2NPs are versatile fluorophores that may be exploited for myriad applications in imaging and analysis. All the reports to date on chemically synthesized PbS_2NPs have explored only their application as a semiconductor material (8, 9), and there are no reports on the fluorescent properties of chemically synthesized PbS_2NPs. Here we report microbially synthesized PbS_2NPs exhibiting fluorescent properties with potential applications in bioimaging.

Conclusion. Lead-based nanomaterials have been extensively reported for various optoelectronic applications due to their size-tunable properties. Among these, the studies on the synthesis of tetragonal β-PbS_2 nanoparticles are very few and employ toxic precursors and extreme conditions of temperature, pressure, and pH for fabrication. In this study, we report the benign synthesis of tetragonal PbS_2NPs by the marine bacterium *Idiomarina* PR58-8 when grown in the presence of 5 mM $Pb(NO_3)_2$ at an ambient temperature of 37°C, an atmospheric pressure (760 mm of Hg), and a neutral pH of 7.0. The nano-preparation exhibited a crystallite domain size of 2.38 nm, a spherical morphology, and an average size distribution of 6 nm. The "as-synthesized" PbS_2NPs exhibited an absorbance maximum at 386 nm and an emission maximum at 570 nm. The emission spectrum of the PbS_2NPs was narrow and symmetric with a Gaussian distribution, and the nanoparticles exhibited a large Stokes' shift with relatively high QY (67%). The fluorescence spectra remained unaffected by the microenvironment of the PbS_2NPs. The particles were found to be noncytotoxic as evidenced by the MTT and ROS assays. The PbS_2NPs were internalized by the HeLa cells and were evenly distributed within the cytoplasm of the cells without penetrating their nuclei. Thus, these nanoparticles can be used for bioimaging applications.

MATERIALS AND METHODS

Materials. All of the chemicals used for the study were of analytical reagent (A.R.) grade and were purchased from HiMedia (India), unless specified. Lead nitrate [$Pb(NO_3)_2$] was prepared as a 1 M stock solution in sterile distilled water (SDW) and filter sterilized.

MIC, growth kinetics, and uptake studies. *Idiomarina* sp. strain PR58-8 was isolated from soil samples of the banks of Mandovi Estuary, Goa, India, as described previously by our laboratory (23) and was used for nanoparticle synthesis. The isolate was grown in ZMB 2216 with various concentrations of

$Pb(NO_3)_2$ (0.05 mM to 10 mM) to determine the MIC. For growth kinetic studies, the bacterium was grown in the presence of $Pb(NO_3)_2$ (0.05, 0.5, 1, and 5 mM). An aliquot of 1 ml was withdrawn every 4 h for up to 60 h, and the optical density was recorded at 600 nm on a UV-visible double-beam spectrophotometer (UV-2450; Shimadzu, Japan). The growth kinetic parameters, such as specific growth rate (μ; h^{-1}), lag time (t_l; min), and doubling time (t_d; min), were determined according to the methods of Berney et al. (48) and Breidt et al. (49). *Idiomarina* PR58-8 grown in the absence of $Pb(NO_3)_2$ served as the control.

Lead uptake by *Idiomarina* PR58-8 was determined using flame atomic absorption spectroscopy (FAAS; Shimadzu AA-700). Aliquots of 5 ml were withdrawn every 6 h from the cultures grown in the presence of 0.5 mM and 5 mM $Pb(NO_3)_2$ for up to 60 h. The cells were separated from the supernatant by centrifugation (10,000 $\times$ *g* for 20 min at room temperature [RT]), and both were digested in 20 ml of 50% nitric acid. Appropriate dilutions of the digested samples were prepared using deionized water, and the samples were subjected to lead quantitation by FAAS. Appropriate controls were also run simultaneously.

Lead-based nanoparticle synthesis. *Idiomarina* PR58-8 was grown in ZMB 2216 in the presence of 5 mM $Pb(NO_3)_2$ at 37°C with shaking at 110 rpm for 60 h. $Pb(NO_3)_2$ was added at either 0 h, i.e., at the time of inoculation, or at 6 h, i.e., in the early exponential phase, to determine the effect of the time of addition on the synthesis of nanoparticles. The cells were harvested by centrifugation (10,000 $\times$ *g* for 20 min at RT), were washed twice with deionized water, and were lysed by sonication (Microson sonicator) at 0°C for three cycles of 1 min each at 3 revolutions per second (rps) (40 W). The cellular debris was separated by centrifugation at 10,000 $\times$ *g* for 40 min. The resulting supernatant was centrifuged at 22,000 $\times$ *g* for 1 h to harvest the nanoparticles. The nanoparticles were washed twice with deionized water and subjected to dialysis against deionized water for 12 h, with changes of water every 2 h. The samples were dried in a hot-air oven at 70°C for 24 h, and the powder was obtained and milled in a mortar and pestle.

For determining the yield of the lead-based nanoparticles, *Idiomarina* PR58-8 was grown in the presence of a requisite amount of $Pb(NO_3)_2$ in duplicate experiments. After the synthesis, the cell pellet was harvested (10,000 $\times$ *g* at RT for 20 min) and processed as follows. One set of cell pellets was used to extract and purify the lead-based nanoparticles and was quantified using FAAS, as described above, to determine the weight/mass of the product (P). The other set of cell pellets was dried and weighed to determine the respective dry weight of the cells (B). The yield with respect to biomass was calculated as Y = P/B, where Y is the yield (μg/mg [dry weight] cells), P is the weight/mass of the product obtained (μg), and B is the dry weight of cells (mg). The yield with respect to substrate provided was determined as SY = P/S, where SY is the yield (mg/mg of Pb), P is the mass/weight of the product (mg), and S is the mass/weight of Pb (substrate; mg) provided to the cells for lead-based nanoparticle synthesis.

Thiol assay. *Idiomarina* PR58-8 was grown in the absence (0 mM/control) and presence of 0.5 mM and 5 mM $Pb(NO_3)_2$. The cells were separated from the supernatant by centrifugation at 10,000 $\times$ *g* at 4°C for 20 min, and the pellets were washed twice with 25 mM Tris-HCl buffer (pH 7.5). Cell-free lysate (CFL) was prepared by sonicating the cells at 0°C for three cycles of 1 min each at three RPS (40 W), and the supernatant obtained after centrifugation (16,000 $\times$ *g* for 45 min at 4°C) was used for the thiol assay. The total thiol (T-SH), non-protein thiol (NP-SH), and protein-bound thiol (PB-SH) were estimated using 5,5′-dithiobis(2-nitrobenzoic acid) (DTNB; Sigma) according to Sedlak and Lindsay (50). The total protein content of the CFL was determined by the method of Bradford (51).

Characterization of the "as-synthesized" nanoparticles. The crystallographic characterization of the nano-preparation was performed on a Rigaku MiniFlex II powder X-ray diffractometer operated at 30 kV/15 mA with Cu K-α (1.54 Å) radiation and a scanning mode of $2\theta/\theta$ continuous scanning. The crystallite domain size was determined using the Debye-Scherrer formula $D = k\lambda/\beta\text{Cos}\theta$, where λ is the wavelength of X-ray applied (1.54 Å), k is the numerical constant with a value of 0.94, $\beta_{1/2}$ is the full width (radians) at half maximum of the signal (2 0 0), and θ is the Bragg angle of signal (2 0 0). The lattice parameters were calculated using the formula $(1/d^2) = [(h^2 + k^2)/d^2] + (l^2/c^2)$, where h, k, and l are Bragg's diffraction planes. The excitation spectra of the lead-based nanoparticles dispersed in deionized water were recorded in the range of 200 to 800 nm using a UV-2450 spectrophotometer. The PL spectra of the sample dispersed in deionized water/DMEM/PBS (pH 7.0) were recorded using a spectrofluorimeter (Jasco FP-6300) with an excitation wavelength of 386 nm. The stability of the preparation was determined by recording the PL spectra of the nanoparticles after storage either as is or as a colloidal suspension for 6 months. A field emission gun transmission electron microscope (FEG-TEM; Technai G2-F30) operated at 300 kV, with a resolution point of 2 Å and angstrom line of 1 Å, was used to obtain high-resolution TEM images and the selected area electron diffraction (SAED) pattern. The nanoparticles were dispersed in deionized water by sonication and were drop-coated on carbon-coated TEM grids for imaging. A field emission gun scanning electron microscope (FEG-SEM; JSM-7600F) equipped with an energy dispersive spectroscope (EDS) operated at 20 keV was used to obtain the elemental composition of the nano-preparation. The band gap energy was calculated using the formula $E(eV) = hc/\lambda$, where hc is 1.24 eV μm and λ is the λ_{abs} obtained by UV-visible spectroscopy (in μm). The quantum yield was measured by the integrated photoluminescence intensities and absorbance values of the lead-based nanoparticles using the reference dye coumarin 153 (QY, 0.58 or 58%). The Stokes' shift was estimated as $\Delta\nu = \nu_{em} - \nu_{abs}$, where $\Delta\nu$ is Stokes' shift in cm^{-1}, ν_{em} is the wavenumber of the emission maxima in cm^{-1}, and ν_{abs} is the wavenumber of the absorbance maxima in cm^{-1}.

Biocompatibility studies. Human epithelial cervical adenocarcinoma (HeLa) cell line obtained from the National Centre for Cell Science (NCCS), Pune, India, was used for these studies. Cells were cultured in DMEM supplemented with 10% fetal bovine serum (FBS) and antibiotics (complete medium [CM]). The

cells were maintained at 37°C in a humidified 5% CO_2 incubator (Sanyo, Japan) and subcultivated according to standard cell culture protocols (52).

The cytotoxicity of the lead-based nanoparticles against the HeLa cell line was determined by a 3-(4,5-dimethyl-2-thiazolyl)-2,5-diphenyl-2H-tetrazolium bromide (MTT) assay. Actively metabolizing cells convert purple MTT dye to pink formazan, which enables an indirect quantification of cell death (53). Exponentially growing cells (5×10^4 cells/well) were seeded in a 24-well plate and allowed to adhere for 24 h. Nanoparticles (10 to 50 μg/ml) were dispersed in DMEM by sonication at 0°C for two cycles of 30 s each at three RPS (40W). The cells were exposed to the nanoparticle dispersion for 24 and 48 h. After exposure, the wells were washed with PBS to remove the nanoparticles, and 30 μl of MTT (5 mg/ml) was added per well. The plate was incubated at 37°C for 4 h in the dark for the formation of the formazan crystals. The crystals were dissolved in 300 μl dimethyl sulfoxide (DMSO), and the absorbances were recorded at 570 nm and 630 nm using a UV-2450 spectrophotometer. Lead nitrate (LN) and lyophilized bacterial cells obtained after cells were grown in the absence of $Pb(NO_3)_2$ designated ML2 (lead-free cell material) were also evaluated for their cytotoxicity toward the HeLa cell line. The cell viability relative to unexposed controls was calculated as % cell viability = $(A_{test}/A_{control}) \times 100$, where, A_{test} is the absorbance of the cells exposed to nanoparticles and $A_{control}$ is the absorbance of cells not exposed to nanoparticles.

Intracellular ROS was estimated using 2′,7′-dichlorofluorescein diacetate (DCFH-DA), a fluorescent probe (54). Exponentially growing cells (5×10^4 cells/well) seeded in 24-well plates were allowed to adhere for 24 h and then exposed to various concentrations of nanoparticles (10 to 50 μg/ml) for a further 24 h. After the exposure, DCFH-DA (20 μM) was added to each of the wells, and the plate was incubated in the dark at 37°C for 30 min. The fluorescence was measured using a JASCO FP-6300 spectrofluorimeter with an excitation wavelength of 485 nm and an emission wavelength of 530 nm. ML2 and LN were also evaluated for their ability to generate ROS in the HeLa cell line. For a positive control, we used 1 μM hydrogen peroxide (H_2O_2).

Nanoparticle internalization and bioimaging. Exponentially growing HeLa cells (5×10^4 cells/well) maintained in CM were seeded onto 2 cm by 2 cm sterile glass slides placed in 6-well plates and were supplemented with 2 ml CM. The cells were allowed to adhere onto the glass slides for 12 h and then incubated with the "as-synthesized" nanoparticles (30 μg/ml) for another 4 h. The slides were washed with sterile PBS (pH 7.0) to remove the excess nanoparticles and other debris and observed using the TRITC filter of an Olympus BX41 epifluorescence microscope. Quantitative fluorescence image analysis was carried out with ImageJ software using the formula CTCF = ID − (A × B), where CTCF is the corrected total cell fluorescence, ID is the integrated density, A is the area of a selected cell, and B is the mean of background fluorescence readings.

Statistical analysis. All of the experiments were carried out in triplicate on different days. The results are expressed as means ± standard errors. Microsoft Excel 2007 software was used for statistical analyses. The differences between the untreated controls and the treated groups for multiple comparisons were determined by one-way analyses of variance (ANOVAs). Two-tailed Student's *t* tests were used to analyze any significant differences between the control and the individual experimental groups. A *P* value of less than 0.05 was considered significant.

ACKNOWLEDGMENTS

We thank SAIF at IIT-Bombay for their help with TEM, HRTEM, and EDAX and A. Chatterjee at the Department of Chemistry, BITS Pilani, K K Birla Goa campus, for her help with spectrofluorometry.

REFERENCES

1. Rao CNR, Cheetham AK. 2001. Science and technology of nanomaterials: current state and future prospects. J Mater Chem 11:2887–2894. https://doi.org/10.1039/b105058n.
2. Xiao G, Wang Y, Ning J, Wei Y, Liu B, Yu WW, Zou G, Zou B. 2013. Recent advances in IV–VI semiconductor nanocrystals: synthesis, mechanism, and applications. RSC Adv 3:8104–8130. https://doi.org/10.1039/c3ra23209c.
3. Patil RS, Pathan HM, Gujar TP, Lokhande CD. 2006. Characterization of chemically deposited nanocrystalline PbS thin films. J Mater Sci 41:5723–5725. https://doi.org/10.1007/s10853-006-0098-4.
4. Wise FW. 2000. Lead salt quantum dots: the limit of strong quantum confinement. Acc Chem Res 33:773–780. https://doi.org/10.1021/ar970220q.
5. Pitcher MW, Cates E, Raboin L, Bianconi PAA. 2000. Synthetic analogue of the biomineralization process: formation of novel lead sulfide phases. Chem Mater 12:1738–1742. https://doi.org/10.1021/cm990465s.
6. Silverman MS. 1966. High-pressure (70-kbar) synthesis of new crystalline lead dichalcogenides. Inorg Chem 5:2067–2069. https://doi.org/10.1021/ic50045a056.
7. Roman-Zamorano JF, Flores Acosta M, Arizpe-Chavez H, Castillon-Barraza FF, Farias MH, Ramirez-Bon R. 2009. Structure and properties of lead and lead sulfide nanoparticles in natural zeolite. J Mater Sci 44:4781–4788. https://doi.org/10.1007/s10853-009-3720-4.
8. Geethu R, Jacob R, Shripathi T, Okram GS, Ganesan V, Tripathi S, Fatima A, Sreenivasan PV, Urmila KS, Pradeep B, Philip RR. 2012. Optoelectronic and thermoelectric properties in Ga doped β-PbS_2 nanostructured thin films. Appl Surf Sci 258:6257–6260. https://doi.org/10.1016/j.apsusc.2012.03.002.
9. Shyju TS, Gopaiakrishnan R. 2013. Studies on lead sulphide thin films deposited by photochemical method, p 340–343. *In* Proceedings of the International Conference on Advanced Nanomaterials & Emerging Engineering Technologies. IEEE, New York, NY.
10. Singh N, Nara S. 2013. Biological synthesis and characterization of lead sulphide nanoparticles using bacterial isolates from heavy metal rich sites. Int J Agric Food Sci Technol 4:16–23.
11. Seshadri S, Saranya K, Kowshik M. 2011. Green synthesis of lead sulfide nanoparticles by the lead resistant marine yeast, *Rhodosporidium diobovatum*. Biotechnol Prog 27:1464–1469. https://doi.org/10.1002/btpr.651.
12. Bai HJ, Zhang ZM. 2009. Microbial synthesis of semiconductor lead sulfide nanoparticles using immobilized *Rhodobacter sphaeroides* Mater Lett 63:764–766. https://doi.org/10.1016/j.matlet.2008.12.050.
13. Kowshik M, Vogel W, Urban J, Kulkarni SK, Paknikar KM. 2002. Microbial synthesis of semiconductor PbS nanocrystallites. Adv Mater 14:815–818.

https://doi.org/10.1002/1521-4095(20020605)14:11<815::AID-ADMA815>3.0.CO;2-K.
14. Shenton W, Douglas T, Young M, Stubbs G, Mann S. 1999. Inorganic–organic nanotube composites from template mineralization of tobacco mosaic virus. Adv Mater 11:253–256. https://doi.org/10.1002/(SICI)1521-4095(199903)11:3<253::AID-ADMA253>3.0.CO;2-7.
15. Walling MA, Novak JA, Shepard JRE. 2009. Quantum dots for live cell and in vivo imaging. Int J Mol Sci 10:441–491. https://doi.org/10.3390/ijms10020441.
16. Wolfbeis OA. 2015. An overview of nanoparticles commonly used in fluorescent bioimaging. Chem Soc Rev 44:4743–4768. https://doi.org/10.1039/C4CS00392F.
17. Chen J, Kong Y, Wang W, Fang H, Wo Y, Zhou D, Wu Z, Li Y, Chen S. 2016. Direct water-phase synthesis of lead sulfide quantum dots encapsulated by β-lactoglobulin for *in vivo* second near infrared window imaging with reduced toxicity. Chem Commun (Camb) 52:4025–4028. https://doi.org/10.1039/C6CC00099A.
18. Wegner KD, Hildebrandt N. 2015. Quantum dots: bright and versatile *in vitro* and *in vivo* fluorescence imaging biosensors. Chem Soc Rev 44:4792–4834. https://doi.org/10.1039/C4CS00532E.
19. Bruchez MJr, Moronne M, Gin P, Weiss S, Alivisatos AP. 1998. Semiconductor nanocrystals as fluorescent biological labels. Science 281:2013–2016. https://doi.org/10.1126/science.281.5385.2013.
20. Chan WCW, Nie S. 1998. Quantum dot bioconjugates for ultrasensitive nonisotopic detection. Science 281:2016–2018. https://doi.org/10.1126/science.281.5385.2016.
21. Bao H, Lu Z, Cui X, Qiao Y, Guo J, Anderson JM, Li CM. 2010. Extracellular microbial synthesis of biocompatible CdTe quantum dots. Acta Biomater 6:3534–3541. https://doi.org/10.1016/j.actbio.2010.03.030.
22. Jacob JM, Lens PN, Balakrishnan RM. 2016. Microbial synthesis of chalcogenide semiconductor nanoparticles: a review. Microb Biotechnol 9:11–21. https://doi.org/10.1111/1751-7915.12297.
23. Seshadri S, Prakash A, Kowshik M. 2012. Biosynthesis of silver nanoparticles by marine bacterium, Idiomarina sp. PR58-8. Bull Mater Sci 35:1201–1205. https://doi.org/10.1007/s12034-012-0417-0.
24. Srivastava P, Kowshik M. 2016. Anti-neoplastic selenium nanoparticles from *Idiomarina* sp. PR58-8. Enzyme Microb Technol 95:192–200. https://doi.org/10.1016/j.enzmictec.2016.08.002.
25. Erten-Unal M, Wixson BG, Gale N, Pitt JL. 1998. Evaluation of toxicity, bioavailability and speciation of lead, zinc and cadmium in mine/mill wastewaters. Chem Spec Bioavailab 10:37–46. https://doi.org/10.3184/095422998782775826.
26. Sauve S, McBride M. 1998. Lead phosphate solubility in water and soil suspensions. Environ Sci Technol 32:388–393. https://doi.org/10.1021/es970245k.
27. Mager EM. 2011. Lead, p 185–236. *In* Wood CM, Farrell AP, Brauner CJ (ed), Homeostasis and toxicology of non-essential metals. Fish physiology, vol 31B. Academic Press, Inc, New York, NY.
28. Nies DH. 1999. Microbial heavy-metal resistance. Appl Microbiol Biotechnol 51:730–750. https://doi.org/10.1007/s002530051457.
29. Jaroslawiecka A, Piotrowska-Seget Z. 2014. Lead resistance in microorganisms. Microbiology 160:12–25. https://doi.org/10.1099/mic.0.070284-0.
30. Harrison JJ, Ceri H, Turner RJ. 2007. Multimetal resistance and tolerance in microbial biofilms. Nat Rev Microbiol 5:928–938. https://doi.org/10.1038/nrmicro1774.
31. Naik MM, Dubey SK. 2013. Lead resistant bacteria: lead resistance mechanisms, their applications in lead bioremediation and biomonitoring. Ecotoxicol Environ Saf 98:1–7. https://doi.org/10.1016/j.ecoenv.2013.09.039.
32. Pages D, Rose J, Conrod S, Cuine S, Carrier P, Heulin T, Achouak W. 2008. Heavy metal tolerance in *Stenotrophomonas maltophilia*. PLoS One 3:e1539. https://doi.org/10.1371/journal.pone.0001539.
33. Kessi J, Hanselmann KW. 2004. Similarities between the abiotic reduction of selenite with glutathione and the dissimilatory reaction mediated by *Rhodospirillum rubrum* and *Escherichia coli*. J Biol Chem 279:50662–50669. https://doi.org/10.1074/jbc.M405887200.
34. Guimaraes-Soares L, Pascoal C, Cassio F. 2007. Effects of heavy metals on the production of thiol compounds by the aquatic fungi *Fontanospora fusiramosa* and *Flagellospora curta*. Ecotoxicol Environ Saf 66:36–43. https://doi.org/10.1016/j.ecoenv.2005.10.005.
35. Fauchon M, Lagniel G, Aude J, Lombardio L, Soulrue P, Petat C, Marguerie G, Sentenac A, Werner M, Labarre J. 2002. Sulfur sparing in the yeast proteome in response to sulfur demand. Mol Cell 9:713–723. https://doi.org/10.1016/S1097-2765(02)00500-2.
36. Qadri SB, Yang JP, Skelton EF, Ratna BR. 1997. Evidence of strain and lattice distortion in lead sulfide nanocrystallites. Appl Phys Lett 70:1020–1021. https://doi.org/10.1063/1.118470.
37. Friedman M, Cuq JL. 1988. Chemistry, analysis, nutritional value, and toxicology of tryptophan in food. A review. J Agric Food Chem 36:1079–1093. https://doi.org/10.1021/jf00083a042.
38. Rover Junior L, Fernandes JC, de Oliveira Neto G, Kubota LT, Katekawa E, Serrano SH. 1998. Study of NADH stability using ultraviolet-visible spectrophotometric analysis and factorial design. Anal Biochem 260:50–55. https://doi.org/10.1006/abio.1998.2656.
39. Truong L, Moody IS, Stankus DP, Nason JA, Lonergan MC, Tanguay RL. 2011. Differential stability of lead sulfide nanoparticles influences biological responses in embryonic zebrafish. Arch Toxicol 85:787–798. https://doi.org/10.1007/s00204-010-0627-4.
40. Hu R, Law WC, Lin G, Ye L, Liu J, Liu J, Reynolds JL, Yong KT. 2012. PEGylated phospholipid micelle-encapsulated near-infrared Pbs quantum dots for *in vitro* and *in vivo* bioimaging. Theranostics 2:723–733. https://doi.org/10.7150/thno.4275.
41. Nozik AJ, Williams F, Nenadovic MT, Rajh T, Micic OI. 1985. Size quantitation in small semiconductor particles. J Phys Chem 89:397–399. https://doi.org/10.1021/j100249a004.
42. Bagga A, Chattopadhyay PK, Ghosh S. 2007. Stokes' shift in quantum dots: origin of dark exciton. *In* Physics of semiconductor devices. Proceedings of the 14th International Workshop on the Physics of Semiconductor Devices, Mumbai, India.
43. Hinds S, Myrskog S, Levina L, Koleilat G, Yang J, Kelley SO, Sargent EH. 2007. NIR-emitting colloidal quantum dots having 26% luminescence quantum yield in buffer solution. J Am Chem Soc 129:7218–7219. https://doi.org/10.1021/ja070525s.
44. Yedjou CG, Milner JN, Howard CB, Tchounwou PB. 2010. Basic apoptotic mechanisms of lead toxicity in human leukemia (HL-60) cells. Int J Environ Res Public Health 7:2008–2017. https://doi.org/10.3390/ijerph7052008.
45. Flora G, Gupta D, Tiwari A. 2012. Toxicity of lead: a review with recent updates. Interdiscip Toxicol 5:47–58. https://doi.org/10.2478/v10102-012-0009-2.
46. Levina L, Sukhovatkin V, Musikhin S, Cauchi S, Nisman R, Bazett-Jones DP, Sargent EH. 2005. Efficient infrared-emitting PbS quantum dots grown on DNA and stable in aqueous solution and blood plasma. Adv Mater 17:1854–1857. https://doi.org/10.1002/adma.200401197.
47. Lidsky TI, Schneider JS. 2003. Lead neurotoxicity in children: basic mechanisms and clinical correlates. Brain 126:5–19. https://doi.org/10.1093/brain/awg014.
48. Berney M, Weilenmann HU, Ihssen J, Bassin C, Egli T. 2006. Specific growth rate determines the sensitivity of *Escherichia coli* to thermal, UVA, and solar disinfection. Appl Environ Microbiol 72:2586–2593. https://doi.org/10.1128/AEM.72.4.2586-2593.2006.
49. Breidt F, Romick TL, Fleming HF. 1994. Rapid method for the determination of bacterial growth kinetics. J Rapid Methods Autom Microbiol 3:59–68. https://doi.org/10.1111/j.1745-4581.1994.tb00308.x.
50. Sedlak J, Lindsay JH. 1968. Estimation of total, protein-bound, and non-protein sulfhydryl groups in tissue with Ellman's reagent. Anal Biochem 25:192–205. https://doi.org/10.1016/0003-2697(68)90092-4.
51. Bradford MM. 1976. A rapid and sensitive method for the quantitation of microgram quantities of protein utilizing the principle of protein-dye binding. Anal Biochem 72:248–254. https://doi.org/10.1016/0003-2697(76)90527-3.
52. Freshney RI. 2010. Subculture and cell lines, p 187–206. *In* Culture of animal cells: a manual of basic techniques and specialized applications. 6th ed. John Wiley and Sons, Inc, New York, NY.
53. van Meerloo J, Kaspers GJ, Cloos J. 2011. Cell sensitivity assays: the MTT assay. Methods Mol Biol 731:237–245. https://doi.org/10.1007/978-1-61779-080-5_20.
54. Mukherjee SG, O'Claonadh N, Casey A, Chambers G. 2012. Comparative *in vitro* cytotoxicity study of silver nanoparticle on two mammalian cell lines. Toxicol In Vitro 26:238–251. https://doi.org/10.1016/j.tiv.2011.12.004.